Letter

Giant interfacial spin Hall angle from Rashba-Edelstein effect revealed by the spin Hall Hanle process

Jing Li,[1,*] Andrew H. Comstock,[2,*] Aeron McConnell,[2] Xin Li,[1] Yu Yun,[1] Dali Sun,[2,†] and Xiaoshan Xu[1,‡]

[1]*Department of Physics and Astronomy and Nebraska Center for Materials and Nanoscience, University of Nebraska, Lincoln, Nebraska 68588, USA*

[2]*Department of Physics and Organic and Carbon Electronics Lab (ORaCEL), North Carolina State University, Raleigh, North Carolina 27695, USA*

(Received 6 September 2023; revised 2 November 2023; accepted 20 November 2023; published 11 December 2023)

The Rashba-Edelstein effect (REE), which generates interfacial spin polarization and subsequent spin current, is a compelling spin-charge conversion mechanism for spintronic applications, since it's not limited by the elemental spin-orbit couplings. In this work we demonstrate REE at Pt/ferroelectric interfaces by showing a positive correlation between polarization and effective spin Hall angle in the recently elucidated spin Hall Hanle effects (SHHE), in which a Larmor precession of spin polarization in a diffusion process from the interface manifest as magnetoresistance and Hall effect. We show that REE leads to a large enhancement of the effective spin Hall angle of ferroelectric interface Pt/h-$LuFeO_3$ compared with that of Pt/Al_2O_3, without obvious differences in the spin relaxation time. Modeling using SHHEs involving REE as an additional source of interfacial polarization suggests that REE can lead to an interfacial spin Hall angle (0.4 ± 0.1) in Pt/h-$LuFeO_3$ that is one order of magnitude larger than the bulk value of Pt. Our results demonstrate that a ferroelectric interface can produce large spin-charge conversion and that SHHEs are a sensitive tool for characterizing interfacial spin-transport properties.

DOI: 10.1103/PhysRevB.108.L241403

Charge-spin current conversion is a fundamental process in spintronics [1]. In general, a charge (spin) current may generate a transverse spin (charge) current via the (inverse) spin Hall effect due to spin-orbit coupling, with a conversion efficiency up to a few percent [2]. With broken inversion symmetry, e.g., at an interface, the gradient of potential energy couples to the spin and generates a preference of spin polarization transverse to the electron momentum [3] and subsequent spin current [Fig. 1(a)], corresponding to the Rashba-Edelstein effect (REE) [4,5]. The charge-spin conversion efficiency induced by REE is not limited by the elemental spin-orbit coupling, which is appealing for spintronic applications. In this regard, it is hypothesized that a metal/ferroelectric interface may have greatly enhanced spin-charge conversion efficiency via REE due to the large interfacial potential gradient, with the advantage of nonvolatile electric-field control [6–9]. On the other hand, determination of REE at metal/ferroelectric interfaces and their spin-transport properties, especially at room temperature, has been challenging because of the lack of direct measurements of the spin polarization [10–13].

Here we reveal the presence of REE in Pt/ferroelectric interfaces by employing the spin Hall Hanle effects (SHHEs) technique [14]. SHHEs, including Hanle magnetoresistance [15,16] (Hanle MR) and Hanle Hall effect [14], have proven successful in quantifying spin-transport parameters, i.e., spin Hall angle θ_{SH}, spin diffusion length λ_s, and spin relaxation time τ_s in Pt films deposited on nonmagnetic insulators, which is free from magnetic proximity effects. As illustrated in Fig. 1(b), SHHEs describe the generation of spin current and accumulation of spin polarization at the Pt/insulator interface via the spin Hall effect (SHE [2,17]), precession of spin polarization in the reflected spin current (Hanle effect [18]), and manifestation of spin precession in MR and Hall effects generated by the inverse spin Hall effect (ISHE [19]). Extra interfacial spin accumulation induced by the presence of REE is expected to modify the Hanle MR and Hanle Hall effect, by which REE can be quantitatively studied.

For ferroelectrics, we focus on hexagonal ferrites and manganites (h-$R$$FeO_3$ and h-$R$$MnO_3$, R = Y, Sc, Ho-Lu) [20,21]. As illustrated in Fig. 1(c), the crystal structure of h-$R$$FeO_3$ and h-$R$$MnO_3$ consists of layers of FeO_5/MnO_5 trigonal bipyramids separated by layers of R ions. With noncentrosymmetric $P6_3cm$ structure, the improper ferroelectricity is induced by the K_3 structural distortion below ~1000 K [21]. Antiferromagnetic orders occur below $T_N \sim 150$ K, with Fe/Mn spins lying mostly in the basal plane [22,23]. The K_3 distortion can be viewed as the collective tilt of the trigonal bipyramids and buckling of the R layer, which leads to a spontaneous polarization along the c axis [24,25]. The larger K_3 distortion in h-$R$$FeO_3$ leads to larger polarization ($\approx 10\ \mu C/cm^2$) [26,27] compared with that of h-$R$$MnO_3$ ($\approx 6\ \mu C/cm^2$) [24,25,28], which provides a way to vary polarization as an independent variable, with Al_2O_3 as the paraelectric control sample. The epitaxial growth of h-$R$$FeO_3$ and h-$R$$MnO_3$ on yttrium

*These authors contributed equally to this work.

†dsun4@ncsu.edu

‡xiaoshan.xu@unl.edu

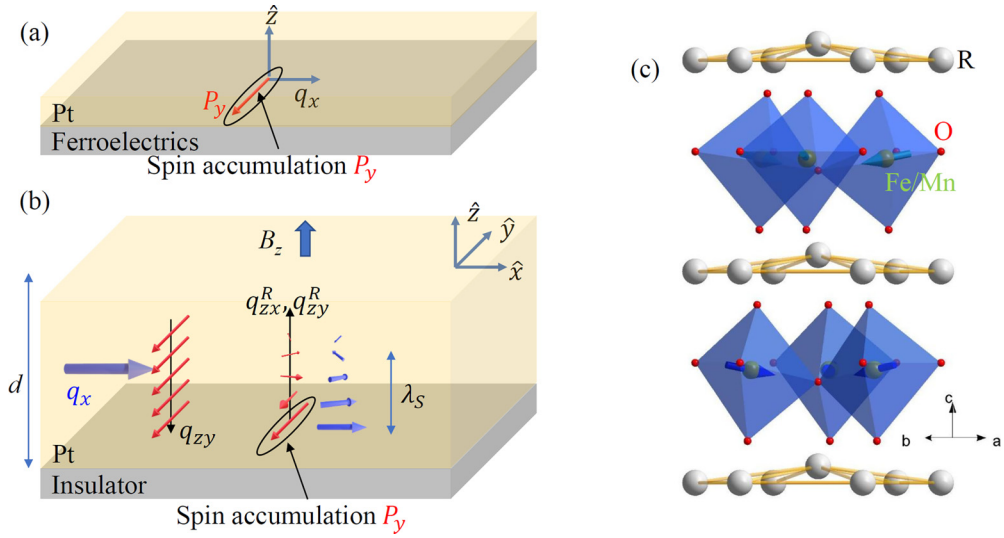

FIG. 1. (a) Schematic of the Rashba-Edelstein effect (REE) in which a charge current q_x at the interface leads to a transverse spin polarization P_y. (b) Schematic of the spin Hall Hanle effects (SHHEs) near a Pt/insulator interface. (A similar process is expected near the Pt/vacuum interface.) q_{zy} is the spin current toward the interface due to q_x and spin Hall effect. An applied magnetic field B_z causes precession of spin polarization P_y during the diffusion from the interface, which results in both q_{zx}^R and q_{zy}^R and manifests in the magnetoresistance and the Hall effect. λ_s and d are spin diffusion length and Pt film thickness, respectively. (c) A unit cell of ferroelectric hexagonal ferrites (manganites) featuring FeO_5 (MnO_5) layers separated by the rare earth layers. Arrows through Fe atoms represent spin orientations.

stabilized zirconia (YSZ) (111) substrates ensures the film quality and minimizes the variation of the control variables such as interfacial roughness [29–31].

We show that the effective spin Hall angle, i.e., spin-charge conversion efficiency, θ_{SH}, at the Pt/ferroelectric interface is largely increased compared to that in Pt/Al_2O_3, while the spin relaxation time remains unchanged. Modeling of the Hanle MR and Hanle Hall effect reveals that REE at the Pt/ferroelectric interface leads to a rescaling of θ_{SH}. The effective spin Hall angle of the $Pt/h\text{-}LuFeO_3$ interface is determined to be one order of magnitude larger than that of bulk Pt.

Pt(111)/h-$LuFeO_3$(001), Pt(111)/h-$YbFeO_3$(001), and Pt(111)/$LuMnO_3$(001) heterostructures were epitaxially grown on YSZ (111) using pulsed laser deposition (PLD), with a yttrium aluminum garnet (YAG) laser (266-nm wavelength, 70-mJ pulse energy over a spot of ≈2 mm diameter, 3-Hz repetition rate). Thin films of h-$LuFeO_3$, h-$YbFeO_3$, and $LuMnO_3$ about 15 nm thick were deposited in 20 mTorr O_2 with 650 °C substrate temperature [23,26] and cooled down in the same pressure to room temperature. After the film-substrate reached room temperature, the chamber was evacuated to 10^{-7} Torr vacuum and the Pt layer of various thickness was deposited *in situ* using the PLD to avoid Pt oxidation [32]. The thicknesses of the Pt layer were measured using x-ray reflectivity. High crystallinity of the oxide films and sharp Pt/oxide interfaces can be inferred from the x-ray diffraction and reflection and atomic force microscopy (see Supplemental Material S1 [33]). The Pt layer was patterned into Hall bar by photolithography and ion milling [14]. Longitudinal (ρ_L) and transverse (ρ_T) resistivity was measured using the Hall bar configuration in the magnetic field applied along different directions at room temperature [14]. Field dependence of ρ_L and ρ_T was symmetrized and antisymmetrized, respectively, to minimize the effects from imperfect sample geometry.

Figure 2 shows the obtained MR (i.e., field dependence of ρ_L) and the Hall effect (i.e., field dependence of ρ_T) in the Pt (5.4 nm)/h-$LuFeO_3$ and the control sample, Pt (5.2 nm)/Al_2O_3

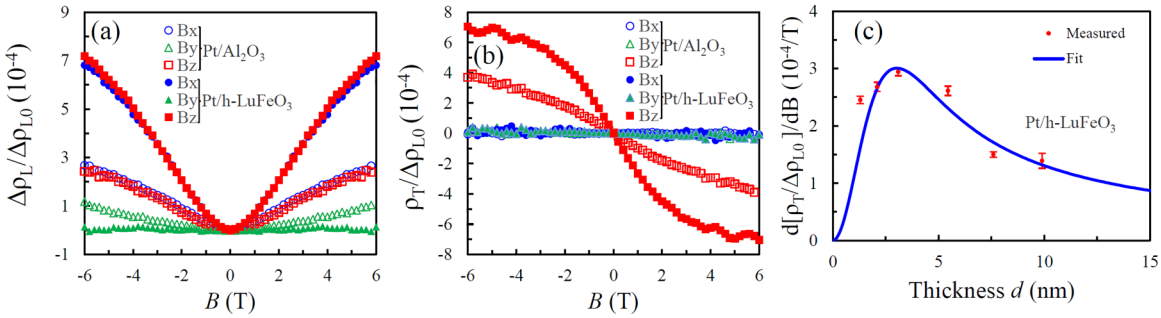

FIG. 2. Field dependence of the normalized longitudinal resistivity (magnetoresistance) (a) and transverse resistivity (Hall effect) of a Pt (5.4 nm)/h-$LuFeO_3$ and a Pt (5.2 nm)/Al_2O_3 sample. (c) Thickness dependence of the low-field (<1 T) slope of the Hall effect for $Pt/h\text{-}LuFeO_3$. The fitting reveals a spin diffusion length $\lambda_s = 0.9 \pm 0.2$ nm.

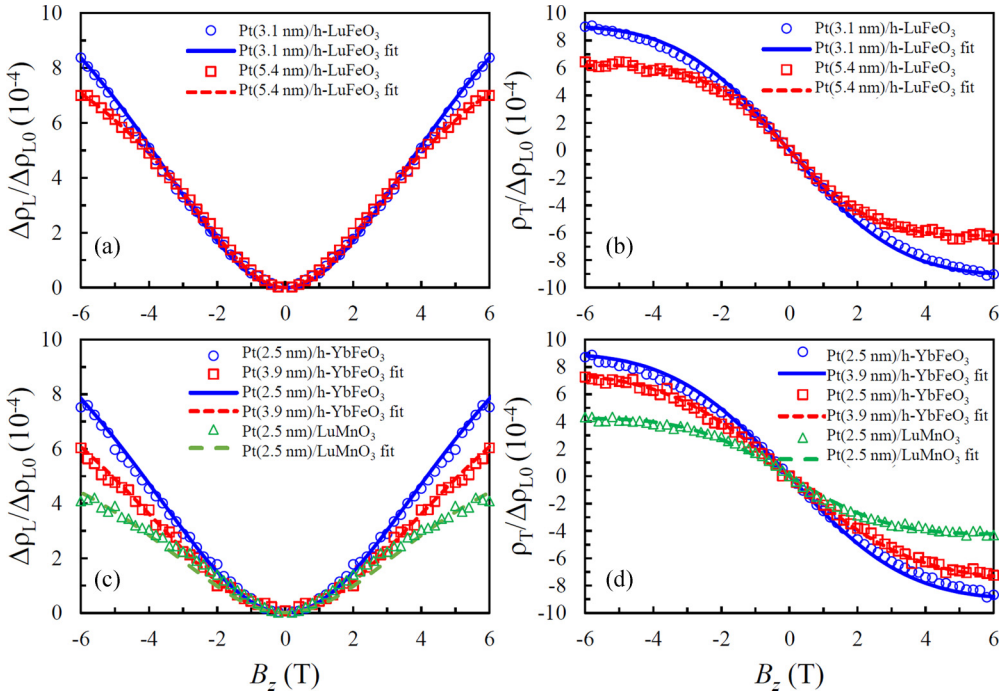

FIG. 3. (a), (c) Measured MR (symbol) as the difference between the magnetoresistance in B_z and that in B_y. (b), (d) The measured Hall effect (symbol). The lines in are fits of the data using the Hanle MR and the Hanle Hall effect according to Eq. (1). For each film, the fit for both MR and Hall effect uses the same set of parameters.

[14]. The MRs in both samples show a symmetry curve that is consistent with reported SHHEs in ρ_L, i.e., MR(B_z) and MR(B_x) are almost identical and much larger than MR(B_y), similar to that of spin Hall magnetoresistance [34–36] but without the presence of magnetic materials. As illustrated in Fig. 1(b), SHHEs include contributions from SHE, Hanle effect, and ISHE: a charge current q_x flowing along the x direction produces a spin current q_{zy} along the z direction toward the Pt-insulator interface, with spin polarization along the y direction via SHE; the precession of spin polarization of the reflected spin current in a magnetic field during the spin diffusion reduces the y component (Hanle effect) and generates the x or z component of the spin polarization; the spin precession shows up in both MR and Hall effect since the reflected spin current generates charge current via the ISHE. Hence, MR(B_x) and MR(B_z) are expected to be larger than MR(B_y), since B_y does not lead to the spin precession. Remarkably, we found that the magnitude of both MR and Hall effect are much larger in Pt(5.4 nm)/h-$LuFeO_3$ than that in Pt(5.2 nm)/Al_2O_3, implying that the spin Hall angle θ_{SH} is substantially larger in Pt/h-$LuFeO_3$.

To determine θ_{SH} in Pt/h-$LuFeO_3$, the spin diffusion length λ_s is needed [14]. Because SHHEs vanish in both thin-film ($d/\lambda_s \to 0$) and thick-film limits ($d/\lambda_s \to \infty$), λ_s can be extracted from the thickness dependence of the SHHE signal. By applying B_z, SHHEs are described using the following equation [14]:

$$\frac{\Delta\rho_{\mathrm{SHHE}}}{\rho_{L0}} = \theta_{\mathrm{SH}}^2 \frac{\tanh(d/2\lambda_s)}{d/2\lambda_s}\left[1 - \frac{1}{\kappa}\frac{\tanh\left(\frac{\kappa d}{2\lambda_s}\right)}{\tanh\left(\frac{d}{2\lambda_s}\right)}\right], \quad (1)$$

where ρ_{L0} is zero-field longitudinal resistivity, d is the film thickness, $\kappa = (1 - i\Omega\tau_s)^{1/2}$ is a complex quantity with $i = \sqrt{-1}$, and $\Omega = g\mu_B B_z/\hbar$ is the Larmor frequency, with g the gyromagnetic factor, μ_B the Bohr magneton, and $\hbar$ the reduced Planck constant. The real and imaginary parts of $\Delta\rho_{\mathrm{SHHE}}$ represent the longitudinal $\Delta\rho_{\mathrm{L,SHHE}}$ and the transverse $\rho_{\mathrm{T,SHHE}}$, respectively. It is shown at the low-field regime, $\rho_{\mathrm{T,SHHE}}$ would be linear to Ω (or B_z) [14]. By fitting the slope of $\rho_{\mathrm{T}}(B_z)$ at the low-field (<1 T) regime [Fig. 2(c)], we found the spin diffusion length as $\lambda_s = 0.9 \pm 0.2$ nm for Pt/h-$LuFeO_3$.

Once λ_s is determined, the spin Hall angle θ_{SH} and spin relaxation time τ_s can be extracted subsequently from the MR $\Delta\rho_L(B_z)$ and Hall effect $\rho_{\mathrm{T}}(B_z)$ simultaneously. As shown in Figs. 3(a) and 3(b), the measured MR and Hall effect can be well fitted using Eq. (1). It is noteworthy that for each sample, the fit for both MR and Hall effect uses the same set of parameters θ_{SH} and τ_s. The extracted θ_{SH} and τ_s are displayed in Figs. 4(a) and 4(b). The obtained θ_{SH} of Pt grown on h-$LuFeO_3$ is roughly three times larger than that of Pt grown on Al_2O_3 [Fig. 4(a)], whereas the difference between τ_s in both systems is much less obvious [Fig. 4(b)].

To verify the correlation between θ_{SH} and polarization, we conducted similar SHHE measurements in Pt/h-$YbFeO_3$ and Pt/$LuMnO_3$ at different Pt thicknesses. While $LuMnO_3$ and h-$YbFeO_3$ are both isomorphic to h-$LuFeO_3$, the former has a substantially smaller polarization, and the latter has a similar polarization compared with that of h-$LuFeO_3$ [24,26,28].

The MR $\Delta\rho_L(B_z)$ and Hall effect $\rho_{\mathrm{T}}(B_z)$ of Pt/h-$YbFeO_3$ and Pt/$LuMnO_3$ are shown in Figs. 3(c) and 3(d). All the curves can be well fitted using Eq. (1); the fitting

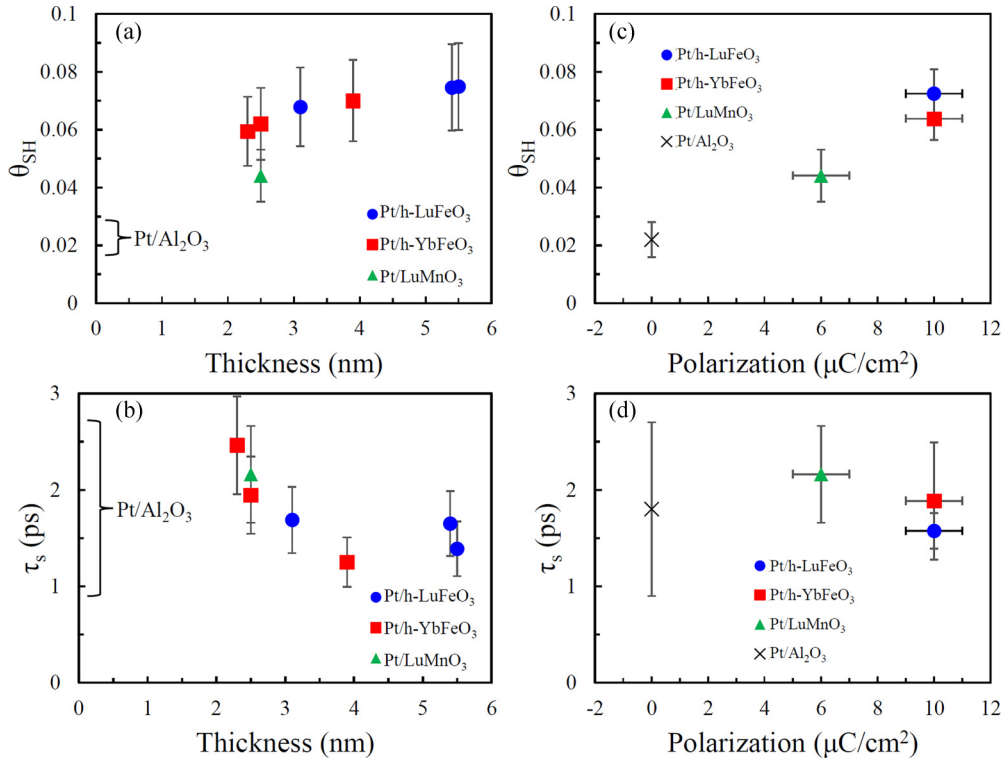

FIG. 4. Spin Hall angle θ_{SH} (a) and spin relaxation time τ_s (b) extracted from the fitting in Fig. 3. The curly brackets indicate the values for Pt/Al_2O_3: $\theta_{SH} = 0.022 \pm 0.006$ and $\tau_s = 1.8 \pm 0.9$ ps. (c) The relations between polarization and θ_{SH}. (d) The relations between polarization and τ_s.

parameters are displayed in Figs. 4(a) and 4(b) for samples of different thickness. Since no obvious thickness dependence is observed, we average θ_{SH} and τ_s with respect to thickness and plot the results against the polarization, as shown in Figs. 4(c) and 4(d) as well as in Table I. A clear positive correlation between polarization and θ_{SH} can be observed, while there is no clear correlation between polarization and τ_s, suggesting that the enhanced θ_{SH} can be attributed to the presence of the ferroelectric interface.

Below we provide a model in which REE at the Pt/ferroelectric interface can lead to the enhancement of θ_{SH}. At the Pt/ferroelectric interface, the large electric potential difference and spin-orbit coupling adds a Rashba term in the Hamiltonian of the itinerant electrons, i.e., $\hat{H}_R \propto \vec{\sigma} \cdot (\vec{p} \times \hat{z})$, where $\vec{\sigma}$, $\vec{p}$, and $\hat{z}$ are the Pauli matrices representing the electronic spin, momentum, and surface normal unit vector [4]. For a charge current with an average momentum $\langle \vec{p} \rangle$ along the x direction, $\langle \vec{p} \rangle \times \hat{z}$ acts like an effective magnetic field along the y direction [4]. This mechanism (or REE) is an extra source of spin accumulation along the y axis at the interface [Fig. 1(a)] which can contribute to the spin current along the z direction via subsequent diffusion [11–13].

TABLE I. Comparison of spin-transport parameters of Pt/Al_2O_3 and that of Pt/hexagonal ferrites and Pt/manganite combined.

	Pt/Al_2O_3	$Pt/h\text{-}LuFeO_3$
Effective spin Hall angle	0.022 ± 0.006	0.072 ± 0.008
Spin diffusion length (nm)	1.63 ± 0.26 nm	0.9 ± 0.2
Spin relaxation time (ps)	1.8 ± 0.9	1.6 ± 0.2

To model the extra spin accumulation via REE, we use the following equations that govern the spin transport near the Pt/ferroelectric interface [37,38]:

$$q_i = -\mu E_i + \theta_{SH} \epsilon_{ijk} q_{jk}, \tag{2}$$

$$q_{ij} = -\mu E_i P_j - D \frac{\partial P_j}{\partial x_i} - \theta_{SH} \epsilon_{ijk} q_k, \tag{3}$$

$$\epsilon_{ijk} P_j \Omega_k + \frac{\partial q_{ki}}{\partial x_k} + \frac{P_i}{\tau_s} - \frac{\beta}{L_R} (\vec{q} \times \hat{z})_i e^{-\frac{2z+d}{2L_R}} = 0, \tag{4}$$

where q_i and q_{ij} (i, $j = x$, y, z) are the components of the charge and spin current density, respectively, in (unified) units of particle per unit time per unit area [37], x_i, Ω_i, P_i, and E_i are the ith component of spatial coordinate, Larmor precession $\vec{\Omega} = g\mu_B \vec{B}/\hbar$, spin polarization density, and electric field, respectively, d, μ, D, and ϵ_{ijk} are film thickness, mobility times carrier density, diffusion coefficient, and antisymmetric matrix, respectively.

Equations (2) and (3) are essentially the "Ohm's law" for charge and spin currents, including the typical drift and diffusion processes, as well as SHE and ISHE [37]. Equation (4) ensures the continuity of spin polarization. The term $-\frac{\beta}{L_R}(\vec{q} \times \hat{z})_i e^{-\frac{2z+d}{2L_R}}$ is introduced to describe the source of spin polarization at the interface ($z = -d/2$) due to REE, where β is a dimensionless coefficient, L_R is the nominal thickness of the interfacial layer, which is presumably much smaller than the film thickness d and spin diffusion length λ_s for Pt. The

top surface is expected to be a Pt-vacuum interface with 100% reflection.

Solving Eqs. (2)–(4) [see Supplemental Material S2] [33] with the boundary conditions $\frac{\partial P_i}{\partial x} = \frac{\partial P_i}{\partial y} = 0$ and $q_{zi}(z = -\frac{d}{2}, \frac{d}{2}) = 0$, we found

$$\frac{\rho_{\mathrm{SHHE}}}{\rho_0} = \theta_{\mathrm{SH}}^2\left(1 + \frac{1}{2}\frac{\beta}{\theta_{\mathrm{SH}}}\right)\frac{\tanh\left(\frac{d}{2\lambda_s}\right)}{\frac{d}{2\lambda_s}}\left[1 - \frac{1}{\kappa}\frac{\tanh\left(\frac{\kappa d}{2\lambda_s}\right)}{\tanh\left(\frac{d}{2\lambda_s}\right)}\right]. \tag{5}$$

Equation (5) differs from Eq. (1) only by a rescaling of $\theta_{\mathrm{SH}}^2 \to \theta_{\mathrm{SH}}^2(1 + \frac{1}{2}\frac{\beta}{\theta_{\mathrm{SH}}})$. In other words, the interfacial Rashba effect can manifest as an enhancement of effective bulk spin Hall angle θ_{SH}. Notice that integration of $\frac{\beta}{L_R}(\vec{q} \times \hat{z})_i e^{-\frac{2z+d}{2L_R}}$ over the entire film thickness ($z = -d/2$ to $d/2$) leads to a spin current βq, suggesting that β is the interfacial spin Hall angle originating from REE. Using $\theta_{\mathrm{SH}} = 0.022 \pm 0.006$ measured from Pt/Al_2O_3 [14] and $\theta_{\mathrm{SH}}\sqrt{1 + \frac{1}{2}\frac{\beta}{\theta_{\mathrm{SH}}}} = 0.072 \pm 0.008$ measured in $Pt/h\text{-}LuFeO_3$ (see Table I), we find $\beta = 0.4 \pm 0.1$, which is about an order of magnitude larger than the bulk spin Hall angle θ_{SH} in Pt.

To compare the charge-spin conversion efficiency in the SHHE process with that in other physical processes like spin pumping [39], we estimate the interface C-S conversion coefficient q_{ICS} as the ratio between the three-dimensional (3D) spin current and two-dimensional (2D) charge current. Essentially, the 2D charge current is the part of the q_x in the interfacial layer $q_x L_R$, and the 3D spin current perpendicular to the interface is found to be $\frac{\beta}{2}q_x$ (see Supplemental Material S2 [33]). Therefore, $q_{ICS} = \frac{1}{2}\frac{\beta}{L_R}$. Again, L_R is the nominal thickness of the interfacial layer and expected to be much smaller than 1 nm. If we assume that $L_{\mathrm{R}} \sim 0.1$ nm, we can estimate that $q_{\mathrm{ICS}} \sim 2\,\mathrm{nm}^{-1}$, which is comparable to the value found for the topological insulator $(Bi_{1-x}Sb_x)_2Te_3$ at 10 K [39].

We note that other factors at the interface may also play a role in the enhancement of θ_{SH}. Hence, quantitative dependence of effective spin Hall angle and REE on polarization as well as effects of other factors call for future investigations.

To summarize, SHHEs are utilized to study the spin accumulation at the Pt/ferroelectric interface due to the Rashba-Edelstein effect, where the ferroelectrics are hexagonal ferrites and manganites. A positive correlation between polarization and effective spin Hall angle and no obvious correlation between polarization and spin relaxation times are found. In particular, a threefold enhancement of effective spin Hall angle was observed in $Pt/h\text{-}LuFeO_3$ compared with that in Pt/Al_2O_3. Modeling using the SHHE process involving the Rashba-Edelstein effect as an additional source of interfacial spin accumulation, the effective interfacial spin Hall angle in $Pt/h\text{-}LuFeO_3$ was extracted as one order of magnitude larger than the bulk value. These results suggest that ferroelectric interfaces are promising for efficient spin-charge interconversion for future spintronic applications.

This research was primarily supported by the U.S. Department of Energy (DOE), Office of Science, Basic Energy Sciences (BES), under Award No. DE-SC0019173. The work at North Carolina State was supported by the U.S. DOE, Office of Science, BES, under Award No. DE-SC0020992. The research was performed in part in the Nebraska Nanoscale Facility: National Nanotechnology Coordinated Infrastructure, and the Nebraska Center for Materials and Nanoscience (and/or NERCF), which are supported by the National Science Foundation under Award No. ECCS: 1542182, and the Nebraska Research Initiative.

[1] I. Žutić, J. Fabian, and S. Das Sarma, Spintronics: Fundamentals and applications, Rev. Mod. Phys. **76**, 323 (2004).

[2] J. Sinova, S. O. Valenzuela, J. Wunderlich, C. H. Back, and T. Jungwirth, Spin Hall effects, Rev. Mod. Phys. **87**, 1213 (2015).

[3] G. Bihlmayer, O. Rader, and R. Winkler, Focus on the Rashba effect, New J. Phys. **17**, 050202 (2015).

[4] F. Hellman, A. Hoffmann, Y. Tserkovnyak, G. S. D. Beach, E. E. Fullerton, C. Leighton, A. H. MacDonald, D. C. Ralph, D. A. Arena, H. A. Dürr, P. Fischer, J. Grollier, J. P. Heremans, T. Jungwirth, A. V. Kimel, B. Koopmans, I. N. Krivorotov, S. J. May, A. K. Petford-Long, J. M. Rondinelli *et al.*, Interface-induced phenomena in magnetism, Rev. Mod. Phys. **89**, 025006 (2017).

[5] V. M. Edelstein, Spin polarization of conduction electrons induced by electric current in two-dimensional asymmetric electron systems, Solid State Commun. **73**, 233 (1990).

[6] M. Fang, W. Zhang, X. Wu, W. Guo, H. Xia, Y. Wang, W. Wang, and J. Shen, Recent advances in tunable spin–orbit coupling using ferroelectricity, APL Mater. **9**, 060704 (2021).

[7] M. Fang, Y. Wang, H. Wang, Y. Hou, E. Vetter, Y. Kou, W. Yang, L. Yin, Z. Xiao, Z. Li, L. Jiang, H. N. Lee, S. Zhang, R. Wu, X. Xu, D. Sun, and J. Shen, Tuning the interfacial spin-orbit coupling with ferroelectricity, Nat. Commun. **11**, 2627 (2020).

[8] P. Noël, F. Trier, L. M. Vicente Arche, J. Bréhin, D. C. Vaz, V. Garcia, S. Fusil, A. Barthélémy, L. Vila, M. Bibes, and J. P. Attané, Non-volatile electric control of spin–charge conversion in a $SrTiO_3$ Rashba system, Nature (London) **580**, 483 (2020).

[9] S. Varotto, L. Nessi, S. Cecchi, J. Sławińska, P. Noël, S. Petrò, F. Fagiani, A. Novati, M. Cantoni, D. Petti, E. Albisetti, M. Costa, R. Calarco, M. B. Nardelli, S. P. Manuel Bibes, R. Bertacco, and C. Rinaldi, Room-temperature ferroelectric switching of spin-to-charge conversion in germanium telluride, Nat. Electron. **4**, 740 (2021).

[10] V. L. Grigoryan, W. Guo, G. E. W. Bauer, and J. Xiao, Intrinsic magnetoresistance in metal films on ferromagnetic insulators, Phys. Rev. B **90**, 161412(R) (2014).

[11] L. Zhou, H. Song, K. Liu, Z. Luan, P. Wang, L. Sun, S. Jiang, H. Xiang, Y. Chen, J. Du, H. Ding, K. Xia, J. Xiao, and D. Wu, Observation of spin-orbit magnetoresistance in metallic thin films on magnetic insulators, Sci. Adv. **4**, 3 (2018).

[12] Z. Chen, P. Chen, Y. Wang, W. Wang, Z. Zhang, X. Lu, R. Liu, X. Fan, G. Yu, and F. Ma, Experimental observation of

interfacial Rashba-Edelstein magnetoresistance in Cr/YIG heterostructures, Phys. Rev. B **107**, 014408 (2023).

[13] Y. Dai, S. J. Xu, S. W. Chen, X. L. Fan, D. Z. Yang, D. S. Xue, D. S. Song, J. Zhu, S. M. Zhou, and X. Qiu, Observation of giant interfacial spin Hall angle in $Y_3Fe_5O_{12}$/Pt heterostructure, Phys. Rev. B **100**, 064404 (2019).

[14] J. Li, A. H. Comstock, D. Sun, and X. Xu, Comprehensive demonstration of spin Hall Hanle effects in epitaxial Pt thin films, Phys. Rev. B **106**, 184420 (2022).

[15] S. Vélez, V. N. Golovach, A. Bedoya-Pinto, M. Isasa, E. Sagasta, M. Abadia, C. Rogero, L. E. Hueso, F. S. Bergeret, and F. Casanova, Hanle magnetoresistance in thin metal films with strong spin-orbit coupling, Phys. Rev. Lett. **116**, 016603 (2016).

[16] H. Wu, X. Zhang, C. H. Wan, B. S. Tao, L. Huang, W. J. Kong, and X. F. Han, Hanle magnetoresistance: The role of edge spin accumulation and interfacial spin current, Phys. Rev. B **94**, 174407 (2016).

[17] A. Hoffmann, Spin Hall effects in metals, IEEE Trans. Magn. **49**, 5172 (2013).

[18] F. J. Jedema, H. B. Heersche, A. T. Filip, J. J. A. Baselmans, and B. J. van Wees, Electrical detection of spin precession in a metallic mesoscopic spin valve, Nature (London) **416**, 713 (2002).

[19] E. Saitoh, M. Ueda, H. Miyajima, and G. Tatara, Conversion of spin current into charge current at room temperature: Inverse spin-Hall effect, Appl. Phys. Lett. **88**, 182509 (2006).

[20] X. Xu and W. Wang, Multiferroic hexagonal ferrites (h-RFeO$_3$,R = Y, Dy-Lu): A brief experimental review, Mod. Phys. Lett. B **28**, 1430008 (2014).

[21] W. Wang, J. Zhao, W. Wang, Z. Gai, N. Balke, M. Chi, H. N. Lee, W. Tian, L. Zhu, X. Cheng, D. J. Keavney, J. Yi, T. Z. Ward, P. C. Snijders, H. M. Christen, W. Wu, J. Shen, and X. Xu, Room-temperature multiferroic hexagonal $LuFeO_3$ films, Phys. Rev. Lett. **110**, 237601 (2013).

[22] M. Fiebig, D. Frohlich, K. Kohn, St. Leute, Th. Lottermoser, V. V. Pavlov, and R. V. Pisarev, Determination of the magnetic symmetry of hexagonal manganites by second harmonic generation, Phys. Rev. Lett. **84**, 5620 (2000).

[23] K. Sinha, H. Wang, X. Wang, L. Zhou, Y. Yin, W. Wang, X. Cheng, D. J. Keavney, H. Cao, Y. Liu, X. Wu, and X. Xu, Tuning the magnetic ordering temperature of hexagonal ferrites by structural distortion, Phys. Rev. Lett. **121**, 237203 (2018).

[24] H. Das, A. L. Wysocki, Y. Geng, W. Wu, and C. J. Fennie, Bulk magnetoelectricity in the hexagonal manganites and ferrites, Nat. Commun. **5**, 2998 (2014).

[25] C. J. Fennie and K. M. Rabe, Ferroelectric transition in $YMnO_3$ from first principles, Phys. Rev. B **72**, 100103(R) (2005).

[26] Y. Yun, P. Buragohain, A. S. Thind, Y. Yin, X. Li, X. Jiang, R. Mishra, A. Gruverman, and X. Xu, Spontaneous polarization in an ultrathin improper-ferroelectric/dielectric bilayer in a capacitor structure at cryogenic temperatures, Phys. Rev. Appl. **18**, 034071 (2022).

[27] K. Sinha, Y. Zhang, X. Jiang, H. Wang, X. Wang, X. Zhang, P. J. Ryan, J.-W. Kim, J. Bowlan, D. A. Yarotski, Y. Li, A. D. DiChiara, X. Cheng, X. Wu, and X. Xu, Effects of biaxial strain on the improper multiferroicity in h-$LuFeO_3$ films studied using the restrained thermal expansion method, Phys. Rev. B **95**, 094110 (2017).

[28] N. Fujimura, T. Ishida, T. Yoshimura, and T. Ito, Epitaxially grown $YMnO_3$ film: New candidate for nonvolatile memory devices, Appl. Phys. Lett. **69**, 1011 (1996).

[29] L. Jin, K. Jia, D. Zhang, B. Liu, H. Meng, X. Tang, Z. Zhong, and H. Zhang, Effect of interfacial roughness spin scattering on the spin current transport in YIG/NiO/Pt heterostructures, ACS Appl. Mater. Interfaces **11**, 35458 (2019).

[30] O. Alves-Santos, E. F. Silva, M. Gamino, R. O. Cunha, J. B. S. Mendes, R. L. Rodríguez-Suárez, S. M. Rezende, and A. Azevedo, Giant spin-charge conversion driven by nanoscopic particles of Ag in Pt, Phys. Rev. B **96**, 060408(R) (2017).

[31] L. Zhou, V. L. Grigoryan, S. Maekawa, X. Wang, and J. Xiao, Spin Hall effect by surface roughness, Phys. Rev. B **91**, 045407 (2015).

[32] Y. Kageyama, Y. Tazaki, H. An, T. Harumoto, T. Gao, J. Shi, and K. Ando, Spin-orbit torque manipulated by fine-tuning of oxygen-induced orbital hybridization, Sci. Adv. **5**, (2019).

[33] See Supplemental Material at http://link.aps.org/supplemental/10.1103/PhysRevB.108.L241403 for more details on structural characterization, transport measurements and analysis, and the model derivations.

[34] Y.-T. Chen, S. Takahashi, H. Nakayama, M. Althammer, S. T. B. Goennenwein, E. Saitoh, and G. E. W. Bauer, Theory of spin Hall magnetoresistance, Phys. Rev. B **87**, 144411 (2013).

[35] H. Nakayama, M. Althammer, Y. T. Chen, K. Uchida, Y. Kajiwara, D. Kikuchi, T. Ohtani, S. Geprägs, M. Opel, S. Takahashi, R. Gross, G. E. W. Bauer, S. T. B. Goennenwein, and E. Saitoh, Spin Hall magnetoresistance induced by a nonequilibrium proximity effect, Phys. Rev. Lett. **110**, 206601 (2013).

[36] S. Husain, N. Figueiredo-Prestes, O. Fayet, S. Collin, F. Godel, E. Jacquet, N. Reyren, H. Jaffrès, and J. M. George, Origin of the anomalous Hall effect at the magnetic insulator/heavy metals interface, Appl. Phys. Lett. **122**, 062403 (2023).

[37] M. I. Dyakonov, *Spin Physics in Semiconductors* (Springer International Publishing AG, Cham, Switzerland, 2017).

[38] M. I. Dyakonov, Magnetoresistance due to edge spin accumulation, Phys. Rev. Lett. **99**, 126601 (2007).

[39] K. Kondou, R. Yoshimi, A. Tsukazaki, Y. Fukuma, J. Matsuno, K. S. Takahashi, M. Kawasaki, Y. Tokura, and Y. Otani, Fermi-level-dependent charge-to-spin current conversion by Dirac surface states of topological insulators, Nat. Phys. **12**, 1027 (2016).